

Large Melting-Point Hysteresis of Ge Nanocrystals Embedded in SiO₂

Q. Xu,^{1,2} I. D. Sharp,^{1,2} C. W. Yuan,^{1,2} D. O. Yi,^{3,2} C. Y. Liao,^{1,2} A. M. Glaeser,^{1,2} A. M. Minor,⁴ J. W. Beeman,² M. C. Ridgway,⁵ P. Kluth,⁵ J. W. Ager III,² D. C. Chrzan,^{1,2} and E. E. Haller^{1,2}

¹Department of Materials Science and Engineering, University of California, Berkeley, California 94720, USA

²Materials Sciences Division, Lawrence Berkeley National Laboratory, Berkeley, California 94720, USA

³Applied Science and Technology, University of California, Berkeley, California 94720, USA

⁴National Center for Electron Microscopy, Lawrence Berkeley National Laboratory, Berkeley, California 94720, USA

⁵Department of Electronic Materials Engineering, Research School of Physical Sciences and Engineering, Australian National University, Canberra ACT 0200, Australia

(Received 4 May 2006; published 9 October 2006; corrected 7 November 2006)

The melting behavior of Ge nanocrystals embedded within SiO₂ is evaluated using *in situ* transmission electron microscopy. The observed melting-point hysteresis is large ($\pm 17\%$) and nearly symmetric about the bulk melting point. This hysteresis is modeled successfully using classical nucleation theory without the need to invoke epitaxy.

DOI: 10.1103/PhysRevLett.97.155701

PACS numbers: 64.60.-i, 61.46.Hk, 64.70.Dv

The melting-freezing transition is the most familiar of phase transitions and has a long history of quantitative study [1,2]. The effect of particle size on the melting point (T_m) of crystals has been studied for nearly a century, beginning with the theoretical work of Pawlow [3] and the first experimental observations of Takagi [4]. Thermodynamic analysis [5] predicts that the difference between the bulk and nanocrystal equilibrium melting points ΔT should vary inversely with particle radius [6–8]:

$$\Delta T \propto \frac{T_m}{Lr} \left[\gamma_{LV} \left(\frac{\rho_S}{\rho_L} \right)^{2/3} - \gamma_{SV} \right], \quad (1)$$

with r the radius of the nanocrystal, T_m the bulk melting point, L the heat of fusion per volume of the solid phase, ρ_L (ρ_S) the density of the liquid (solid) phase, and γ_{LV} (γ_{SV}) the energies of the liquid-vapor (solid-vapor) interfaces. For most materials, $\Delta T < 0$, and experimentally it is common to see nanocrystals with $\Delta T = -300$ K [6,9].

Experimental observations of melting and freezing, however, are often influenced by the kinetics of the nucleation of the liquid and solid phases, respectively. Lindemann [10] predicted that melting begins when the amplitude of the vibrational motions in the lattice exceeds a certain threshold value. Surface atoms are less strongly bound, suggesting that melting should begin at the surface, and this picture is supported by recent molecular dynamics simulations of metal nanocrystals [11]. The phenomena of superheating (an observed T_m above the bulk equilibrium value) and supercooling (an observed T_m below the bulk equilibrium value) are thus intimately tied to the solid-vapor, liquid-vapor, and liquid-solid interface energies (γ_{SV} , γ_{LV} , and γ_{LS} , respectively) [12]. If $\gamma_{LV} < \gamma_{LS} + \gamma_{SV}$, a solid phase will not nucleate at the surface, and it may be possible to supercool the liquid phase. In principle, if $\gamma_{SV} < \gamma_{LS} + \gamma_{LV}$, the surface will not premelt and it will be possible to superheat a solid. For bulk materials, the first inequality holds but not the second [12]. Hence, one

can often supercool a bulk liquid with free surfaces but not superheat a bulk solid under the same conditions.

Size-dependent kinetic barriers to melting of freestanding nanocrystals were first considered quantitatively by Couchman and Jesser [7]. They calculated the free energy of a melting particle as a function of the thickness of the molten outer layer. As this layer increases in thickness, the free energy passes through a maximum, creating a kinetic barrier to melting. The experimentally observed melting point is deduced from the nucleation rate for the transition.

Consideration of embedded nanocrystals greatly expands the range of possible behaviors and allows for complete study of the melting-point hysteresis. From a classical thermodynamics perspective, there are two major differences between the freestanding and embedded nanocrystal cases. First, the interface energies involved in the melting process differ between the two configurations. In fact, the liquid-vapor and solid-vapor interfaces may no longer be relevant to the melting process and may be replaced by the liquid-matrix and solid-matrix interface energies. Second, the geometric constraints implied by embedding might lead to different equilibrium and kinetic behaviors.

There are a handful of prior experimental observations of superheating (relative to bulk melting points) of embedded nanocrystals [13–18]. A common feature of most of these studies is the suggestion that interface epitaxy suppresses the vibrational motion of the surface atoms, thus limiting surface premelting and increasing the melting point in accord with the Lindemann criterion. This notion has been incorporated into a phenomenological model for melting [19]. From this perspective, then, it is interesting to consider the melting of nanocrystals confined to an amorphous matrix where epitaxy is not possible.

We performed electron diffraction on Ge nanocrystals embedded in silica formed using the process reported earlier [20]. This process results in a nearly Gaussian distribution of nearly spherical nanocrystals with an average radius of 2.5 nm and an rms deviation of 1.3 nm. We note

that freestanding nanocrystalline Ge shows the typical melting-point depression found for most materials [21].

Electron diffraction was used to study the melting behavior of the embedded nanocrystals. Here the melting temperature is defined as the temperature at which the disappearance of the diffraction pattern occurs, indicating the loss of lattice order. The *in situ* heating and cooling experiments were performed inside a JEOL 3010 transmission electron microscope operating at 300 kV. A plan-view specimen was prepared by backthinning the Si substrate and leaving the implanted silica film side untouched. The 200–300 nm thick specimen was then placed in the Gatan Ta628 holder, which contains a tantalum furnace and a pair of calibrated thermocouples. The lowest possible electron beam intensity was used to prevent beam heating. We see no degradation of the sample due to *e*-beam effects. Diffraction experiments on Au nanocrystals embedded in SiO₂ fabricated through ion beam synthesis were employed to confirm the accuracy of the experimentally measured temperatures. Measurements of their melting point with our experimental approach yielded a melting point in good agreement with expectations.

Several heating-cooling cycles were performed in steps of 15 K per 5 min from room temperature to 1470 K on three Ge nanocrystal specimens. (The nanocrystal coarsening rate was negligible.) All cycles gave identical results. The melting and crystallization were characterized by the intensity change of the diffraction peaks in the selective area diffraction patterns obtained on a 0.2 μm^2 field of embedded nanocrystals. The ring patterns were recorded by a Gatan optically coupled TV-rate CCD camera and integrated circumferentially about the pattern center to produce the reported diffracted intensity.

Electron diffraction patterns obtained while heating Ge nanocrystals in SiO₂ from ambient temperature to 1450 K are shown in Fig. 1. The 111, 202, and 113 diffraction peaks persist to 1400 K, nearly 200 K above the bulk melting point (1211 K). Figure 2 displays diffracted intensities as a function of temperature for heating and cooling cycles, for Ge nanocrystals embedded in silica. Melting starts at 1350 K and is complete by 1450 K; resolidification begins at 980 K and is complete by 880 K. This corresponds to a hysteresis loop approximately 470 K wide and centered approximately on T_m .

The observation of a large hysteresis ($\pm 17\%$ of T_m) nearly symmetric about the bulk melting point is unusual and surprising. The only similar observation of which we are aware is the case of Sn nanocrystals embedded in carbon nanostructures [18]. However, it is demonstrated here that a simple, classical thermodynamics-based model is consistent with all of our experimental observations.

There are two theoretical aspects that need to be addressed in the development of a model for the melting of confined nanoparticles. One must develop a theory for the equilibrium melting point, and one must develop a theory for the kinetics of melting. In developing a kinetic theory, one must construct the proper kinetic pathway. This path-

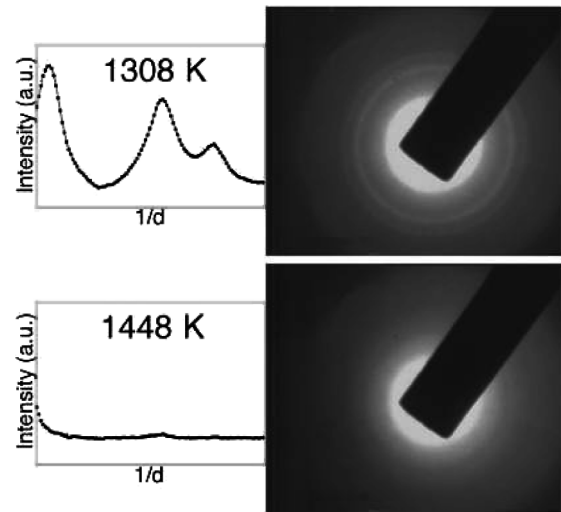


FIG. 1. Diffraction patterns and integrated intensity plots obtained during measurements of the Ge melting point. 1308 K is 97 K above the bulk melting point of Ge, and diffraction rings are clearly observed.

way will be dictated by the geometry of the embedded nanocrystal and the relevant interface energies.

Determination of the equilibrium melting point requires a model for the change in free energy upon melting. There are three contributions to consider: the change in bulk free energy, the change in interface free energy, and the change in strain energy upon melting. The change in bulk free energies can be related to the latent heat in the standard manner (for T near T_m). The changes in strain and interface energies pose a more formidable theoretical problem.

The density of Ge increases 4.6% upon melting, suggesting that melting may lead to the formation of a gap between the molten droplet and the matrix. Based on the

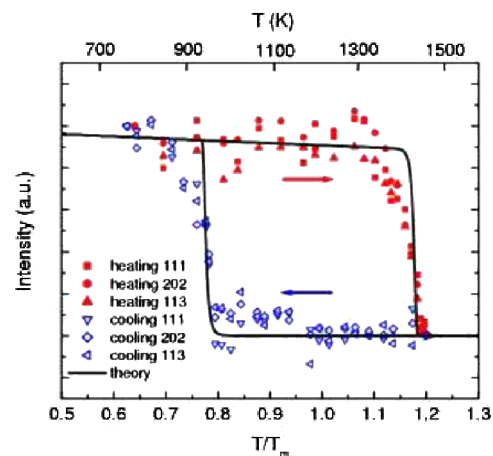


FIG. 2 (color online). Intensity of the 111, 202, and 113 Ge diffraction rings as a function of temperature during heating (solid symbols) and cooling (open symbols). Both superheating and supercooling are clearly observed. The solid curve is the prediction of the kinetic theory presented in the text. All temperature measurements are uncertain to ± 15 K.

density change, a 2.5 nm radius molten sphere will have an average gap of 0.4 Å between its surface and the matrix (barring the effects of thermal expansion). Within a continuum theory, the fate of this gap depends upon the values of γ_{LM} , γ_{LV} , and γ_{SV} , and the change in strain energy associated with the suppression or formation of a gap. (Here L indicates liquid Ge, S solid Ge, M the SiO_2 matrix, and V vapor.) Formation of a gap creates LV and MV interfaces at the expense of the LS interface. Suppression of gap formation puts the liquid Ge in tension, shears the SiO_2 matrix, and might lead to an overall increase in elastic energy. To make further progress, one needs estimates of the interface and strain energies.

The interface energies used on the analysis are given in Table I. These values, with the exceptions of γ_{LS} and γ_{SM} , are extrapolated from values in the literature or deduced from other experiments independent of the present melting-point measurements. Applying the kinetic model described below to the description of the experimental data establishes that $|\gamma_{SM} - \gamma_{LM}| \lesssim 0.05 \text{ J m}^{-2}$ and $\gamma_{LS} = 0.26 \pm 0.03 \text{ J m}^{-2}$. This latter value differs from that quoted by Turnbull [26]. However, Turnbull's analysis employed a calculated heat of fusion L that differs from more recent estimates. After the appropriate scaling, Turnbull's value becomes $\gamma_{LS} = 0.23 \text{ J m}^{-2}$, in reasonable agreement with our value.

The surface energies listed in Table I imply that the solid Ge/ SiO_2 interface will not premelt because $\gamma_{LM} + \gamma_{LS} > \gamma_{SM}$. Further, the molten phase will not "presolidify" at the interface because $\gamma_{SM} + \gamma_{LS} > \gamma_{LM}$. Thus, the solid-liquid transformation will require nucleation in both directions. Finally, supercooling but not superheating of bulk Ge is predicted.

Based on these interface energies, the opening of a gap would increase the surface energy of a nanocrystal 5 nm in diameter by between 50 and 150 eV. This increase in surface energy would have to be countered through a reduction in strain energy. In the absence of a gap, the liquid would be placed under tension and be strained approximately 1%. Assuming that the bulk modulus of the liquid is 77 GPa, the interface stress is 1 J m^{-2} , using accepted values for all other parameters, and, applying the formal-

ism in Ref. [27], the associated elastic strain energy is estimated to be 6 eV. Thus, the increase in surface energy associated with opening a gap is expected to be an order of magnitude larger than the total strain energy of the liquid phase. In this continuum picture, a gap will not open.

With these values for the surface energies and neglect of the elastic energy, one can compute two useful quantities for the confined Ge nanocrystals. First, by comparing the free energies of isolated embedded molten and solid nanocrystals, an estimate for the equilibrium melting point can be ascertained. Specifically, we find an expression similar to that of Couchman and Jesser [7] for the change in the equilibrium melting point:

$$\Delta T = \frac{3T_m}{Lr} [\gamma_{LM} - \gamma_{SM}]. \quad (2)$$

For our choice of parameters, $\Delta T = 0 \text{ K}$.

Second, we can compute an approximate rate for melting and solidification of the confined Ge nanocrystals. This rate is computed using a traditional nucleation theory. A kinetic pathway is identified, the free energy barrier associated with following that pathway is computed, and the transition rate is then governed by Boltzmann statistics. The energy barriers are computed by first solving for the equilibrium geometry of the nucleus as a function of liquid volume and then computing the change in free energy as a function of nucleus size. The maximum in the free energy vs nucleating phase volume fraction plot yields the energy barrier that must be overcome in order to melt or solidify the nanocrystal. Figures 3(a)–3(d) display select configurations along the kinetic pathway for a nanocrystal with $r = 2.5 \text{ nm}$. The kinetic theory assumes an attempt frequency per atom of 10^{11} sec^{-1} , that nucleation is heterogeneous at the Ge/ SiO_2 interface, and that a nucleation rate of 1 sec^{-1} is experimentally observable. Figure 3(a) is the predicted critical nucleus for the melting of 2.5 nm radius nanocrystal, and Fig. 3(d) is the critical nucleus associated with solidifying that same nanocrystal. The corresponding predicted superheating and supercooling temperatures are 199 K above and 256 K below the bulk melting point of Ge, respectively. The energy barrier to melting is 3.91 eV, and that associated with solidification is 2.65 eV.

The predicted kinetically determined melting temperatures for nanocrystals are plotted in Fig. 3(f). These melting-point predictions are then combined with a simple kinetic model for diffraction to model the experimental results. Specifically, the diffracted intensity from each nanocrystal is assumed to scale with the sixth power of the radius and is corrected for Debye-Waller effects by extrapolating known sub-melting-point behavior [28]. The individual nanocrystal melting-point predictions are convoluted with the measured nanocrystal size distribution [20], and the diffracted intensity from the nanocrystals that are solid at each temperature is reported in Fig. 2. The agreement between experiment and theory is excellent, though it is noted that the behavior of the predicted intensity is dominated by nanocrystals with $r \gtrsim 2 \text{ nm}$.

TABLE I. Interface energies employed in the kinetic model of melting.

Interface	Interface energy (J m^{-2})	Notes
LS	0.26	Determined from present experiments
LV	0.59	Extrapolated from experiment [22]
SV	1.0	References [23,24]
LM	0.7–0.9	Reference [22]
SM	0.7–0.9	Determined from present experiments
MV	0.41	Extrapolated from Ref. [25] data

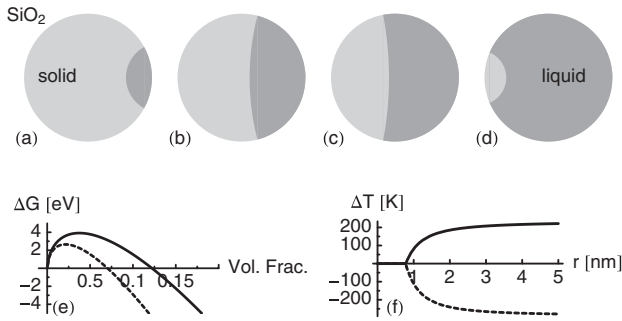


FIG. 3. (a)–(d) The kinetic pathway used to compute the transformation rate. A spherical particle of Ge is embedded in an SiO₂ matrix. The nanocrystal is shown in cross section and is assumed axially symmetric about an axis pointing from left to right. (e) Free energy curves associated with melting (solid line) and solidification (dashed line) at the kinetically determined melting points for a nanocrystal with $r = 2.5$ nm. The x axis represents the volume fraction of the nucleating phase. (f) The predicted melting (solid line) and solidification (dashed line) points plotted vs nanocrystal radius.

The model makes clear which surface tensions drive the observed behavior. The change in equilibrium melting point is determined by the difference $\gamma_{LM} - \gamma_{SM}$. This quantity also impacts the centering of the hysteresis, as it determines the geometry of the *SLM* triple junction. For $\gamma_{LM} - \gamma_{SM} = 0$, the contact angle is $\pi/2$, and the hysteresis loop will be nearly symmetric about the bulk melting point. The width of the hysteresis loop is governed by γ_{LS} . Note that the model also assumes the Ge/SiO₂ interfaces to be smooth. It is possible that the formation of a very thin Ge-oxide layer between the Ge and SiO₂ might lead to a sufficiently smooth interface.

These experiments demonstrate clearly the advantages of studying embedded nanocrystals. First and foremost, the embedded structure allows for complete study of the melting-point hysteresis. Therefore, one can assess the relative importance of kinetically limited and equilibrium behaviors directly. Further, the embedded geometry enables the engineering of interface energies and expands substantially the scope of observable melting-point behavior.

In conclusion, Ge nanocrystals embedded in SiO₂ are shown to have a melting-point hysteresis nearly 470 K wide and centered nearly on the bulk melting point. This initially surprising result is explained naturally using classical nucleation theory and bulk materials parameters.

The authors acknowledge A. Robinson and N. Phillips for their insightful critique of this manuscript. D. C. C. and E. E. H. acknowledge support from the Miller Institute for Basic Research in Science. M. C. R. and P. K. acknowledge support from the Australian Research Council. This work is supported in part by the Director, Office of Science, Office of Basic Energy Sciences, Division of Materials Science and Engineering, of the U.S. Department of

Energy under Contract No. DE-AC02-05CH11231 and in part by U.S. NSF Grant No. DMR-0405472. Electron microscopy was performed at the National Center for Electron Microscopy, LBNL.

- [1] R. W. Cahn, *Nature (London)* **323**, 668 (1986).
- [2] R. W. Cahn, *Nature (London)* **413**, 582 (2001).
- [3] P. Pawlow, *Z. Phys. Chem., Stöchiom. Verwandtschaftsl.* **65**, 1 (1909).
- [4] M. Takagi, *J. Phys. Soc. Jpn.* **9**, 959 (1954).
- [5] K. J. Hansen, *Z. Phys.* **157**, 523 (1960).
- [6] P. Buffat and J.-P. Borel, *Phys. Rev. A* **13**, 2287 (1976).
- [7] P. R. Couchman and W. A. Jesser, *Nature (London)* **269**, 481 (1977).
- [8] F. Baletto and R. Ferrando, *Rev. Mod. Phys.* **77**, 371 (2005).
- [9] A. N. Goldstein, C. M. Echer, and A. P. Alivisatos, *Science* **256**, 1425 (1992).
- [10] F. A. Lindemann, *Z. Phys.* **11**, 609 (1910).
- [11] Y. Qi, T. Cagin, W. L. Johnson, and W. A. Goddard III, *J. Chem. Phys.* **115**, 385 (2001).
- [12] L. D. Landau and E. M. Lifshitz, *Statistical Physics Part I* (Pergamon, Oxford, 1980).
- [13] C. J. Rossouw and S. E. Donnelly, *Phys. Rev. Lett.* **55**, 2960 (1985).
- [14] J. Dages, H. Gleiter, and J. H. Perepezko, *Mater. Res. Soc. Symp. Proc.* **57**, 67 (1986).
- [15] L. Grabaek, J. Bohr, H. H. Andersen, A. Johansen, E. Johnson, L. Sarholt-Kristensen, and I. K. Robinson, *Phys. Rev. B* **45**, 2628 (1992).
- [16] O. S. Mei, S. C. Wang, H. T. Cong, Z. H. Jin, and K. Lu, *Phys. Rev. B* **70**, 125421 (2004).
- [17] Z. Zöllmer, K. Rätzke, F. Faupel, and A. Meyer, *Phys. Rev. Lett.* **90**, 195502 (2003).
- [18] F. Banhart, E. Hernández, and M. Terrones, *Phys. Rev. Lett.* **90**, 185502 (2003).
- [19] Q. Jiang, Z. Zhang, and J. C. Li, *Chem. Phys. Lett.* **322**, 549 (2000).
- [20] I. D. Sharp, D. O. Yi, C. Y. Liao, J. W. Beeman, Z. Liliental-Weber, K. Yu, D. N. Zakharov, J. W. Ager III, D. C. Chrzan, and E. E. Haller, *Appl. Phys. Lett.* **86**, 063107 (2005).
- [21] N. T. Gladkich, R. Neidermayer, and K. Spiegel, *Phys. Status Solidi* **15**, 181 (1966).
- [22] N. Kaiser, A. C. F. R. Szofran, S. D. Cobb, and K. W. Benz, *J. Cryst. Growth* **231**, 448 (2001).
- [23] M. Albrecht, P. O. Hansen, S. Christiansen, W. Dorsch, H. P. Strunk, and E. Bauser, *Scanning Microsc.* **8**, 925 (1994).
- [24] R. J. Jaccodine, *J. Electrochem. Soc.* **110**, 524 (1963).
- [25] A. Roder, W. Kob, and K. Binder, *J. Chem. Phys.* **114**, 7602 (2001).
- [26] D. Turnbull, *J. Appl. Phys.* **21**, 1022 (1950).
- [27] J. W. Cahn and F. Larche, *Acta Metall.* **30**, 51 (1982).
- [28] V. F. Sears and S. A. Shelley, *Acta Crystallogr. Sect. A* **47**, 441 (1991).